Solar Energy 271 (2024) 112423

Contents lists available at ScienceDirect

Solar Energy

journal homepage: www.elsevier.com/locate/solener

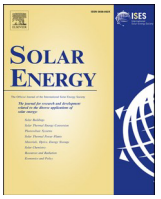

Bulk ceramics of lanthanum hexaboride with enhanced spectral selectivity and photothermal efficiency for novel hybrid thermal-thermionic solar absorbers

Elisa Sani [a,*,1], Diletta Sciti [b], Simone Failla [b], Alessandro Bellucci [c], Matteo Mastellone [c], Stefano Orlando [d], Daniele M. Trucchi [c]

[a] CNR-INO, National Institute of Optics, Largo E. Fermi, 6, I-50125 Firenze, Italy
[b] CNR-ISSMC, Institute of Science, Technology and Sustainability for Ceramics, Via Granarolo 64, I-48018 Faenza, Italy
[c] CNR-ISM, Institute of Structure of Matter - Montelibretti Section, Via Salaria km 29.300, I-00015 Monterotondo Scalo (Rome), Italy
[d] CNR-ISM, Institute of Structure of Matter – Tito Scalo Section Zona Industriale, I-85050 Tito (PZ), Italy

ARTICLE INFO

Keywords:
Surface texturing
Solar absorbers
Concentrated solar radiation
Solar-to-electric conversion
Spectrally selective solar absorbers
High temperature

ABSTRACT

Lanthanum hexaboride (LaB_6) single-crystals are known from a long time for their excellent thermionic and field-assisted electron-emitting properties. Recently, multi-crystalline ceramics, which offer several technological advantages over single-crystals, have been studied as well, proving a low work function and Richardson constant, in addition to favorable optical properties for high-temperature solar radiation absorbers. However, to fully disclose to LaB_6 ceramics the novel application of a double-function bulk thermionic emitter, enabled by the direct absorption of solar radiation, and, at the same time, thermodynamic solar absorber for Concentrating Solar Power (CSP), their optical properties should be further optimized. The ideal result, consisting in the selective increase of the solar absorptance and decrease of the thermal emittance, thus increasing both the spectral selectivity and the photothermal efficiency of the absorber, has been obtained in this work by realizing Laser-Induced Periodic Surface Structures (LIPSS) on the ceramic surface by means of femtosecond-laser treatments. LIPPS formation has been investigated as a function of the accumulated laser fluence.

1. Introduction

Concentrating Solar Power (CSP) and Concentrating Solar Thermal (CST) are two related technologies based on mirrors (mainly, or on lenses) which focus the solar radiation onto a small area, where an absorber material is heated, reaching high temperatures (>300 °C). The heat can be used either to produce electricity using turbines (in CSP) or used as process heat (in CST). Both systems can be designed with different solar-concentrating architectures, among which the solar tower emerged as one of the most promising, due to higher temperature operation and easier integration of direct thermal storage [1]. Concentrating solar technologies are a key tool for the green energy transition. For instance, for CSP, recent IEA projections [2] foresee an installed capacity of 281 GW by 2040 and 426 GW by 2050 in the Net Zero Emissions by 2050 Scenario (NZE). As for CST, it is rapidly raising expectations both to decarbonize energy-intensive sectors (e.g. cement, steel, ceramics, desalination) by supplying process-heat and to renewably synthesize chemicals and fuels for industry and transportation [3–5]. The key technological leap for increased penetration of both CSP and CST is a high operating temperature > 550 °C, as it boosts the efficiency of power thermodynamic cycles and enables endothermic, high-temperature, chemical reactions.

In this context, Ultra-High Temperature Ceramics (UHTCs), which include borides and carbides of early transition metals, have been proposed as novel high-temperature bulk solar absorbers and extensively studied by our group [6,7]. UHTCs are known for their extremely high melting temperature, high thermal conductivity and excellent stability at high temperatures, making them the election materials for thermal shields in aerospace applications (re-entry vehicles, nose cones, rocket nozzles). Among UHTCs, borides are characterized by a superior oxidation resistance [8]. Our previous works have proven that they also possess favorable optical properties for solar applications, in particular

* Corresponding author.
E-mail address: elisa.sani@ino.cnr.it (E. Sani).
[1] ORCID ID: 0000-0001-9854-2892.

https://doi.org/10.1016/j.solener.2024.112423
Received 3 November 2023; Received in revised form 15 January 2024; Accepted 20 February 2024
Available online 24 February 2024

the spectral selectivity and low thermal emittance [9] in contrast to silicon carbide, which is currently the most advanced material used in CSP. On the other hand, if the solar absorptance of borides is concerned, it can typically be improved, e.g. by acting on the surface roughness and/or porosity [10,11]. These approaches, however, typically also increase the thermal emittance. A useful approach towards application-optimized materials is realizing a surface texturing, e.g. by chemical etching [12] or laser processing [13]. This latter, once suitably optimized, has been recently proven to be able to provide a selective enhancement of solar absorptance, not only with a limited increase of thermal emittance, so that the photothermal efficiency of the absorber is enhanced [14], but with an emittance decrease, instead [15], which translates in a superior spectral selectivity as well.

Lanthanum hexaboride (LaB_6) is known from a long time for its excellent capability of thermionic and field-assisted electron emission [16], thanks to high thermal stability and low work function, such to be deeply exploited in several electron emission applications, like electron guns in cathode tubes [17] or in electron microscopes [18].

Recently, we have reported on optical and thermionic emission properties of sintered LaB_6 multi-crystalline ceramics to evaluate their potential as solar absorber material for CSP systems [19], as well as for high-temperature thermionic energy converters (TECs) [20], showing, for these ceramics, competitive solar absorptance and spectral selectivity and promising low work function and Richardson constant. However, our previous studies highlighted some key points to be improved in view of the development of a *double-function active* solar absorber *also* acting as a cathode material for solid-state converters in a CSP architecture (i.e., a double-function high-temperature thermodynamic solar-absorber *and* thermionic solar generator). Indeed, we found that to obtain a remarkable solar-to-electric direct conversion efficiency, even able to surpass 35 %, a proper ceramic surface engineering would be carried out to selectively increase the solar absorptance, without detrimentally enhancing the thermal emittance [20]. This can be obtained through the selective trapping of desired radiation wavelengths by a proper surface texturing, as shown in the literature for different materials including, besides UHTC ceramics [13], bulk semiconductors [21], semiconductors films [22] and metallic [23] or dielectric coatings deposed on metal substrates [24]. For ultra-hard materials, like the case of borides, the use of ultra-short laser machining emerged as one of the better investigated and most promising methods to produce surface textures [25]. However, for lanthanum hexaboride, femtosecond laser processing has been used so far only for the fabrication of field-emission tip arrays to improve the already high emission capability of LaB6 [26]. Instead, to the best of our knowledge, no attempts of creating Laser-Induced Periodic Surface Structures (LIPSS) have been reported for this boride. LIPSS, e.g. a regular system of periodic morphological patterns is formed usually after irradiation with ultrashort linearly polarized laser pulses and were discovered in the 60 s on laser treated germanium [27]. Since then, systematic studies in metals [28], semiconductors and dielectrics [29] have been conducted to understand the main parameters that influence the final surface morphology. The most accepted explanation for the origin of these structures is based on the interference of the incident laser radiation with electromagnetic surface waves that propagate or scatter at the surface of the irradiated material. LIPPS formation can be exploited to obtain a surface functionalization that has application in many fields, including optics, tribology, and biomedicine [30].

Therefore, in the present work we realized different texturing treatments on a pure and porous LaB_6 ceramic sample using a femtosecond laser and setting different laser parameters, and we systematically characterized the optical properties of obtained surfaces. We show that, depending on the laser processing parameters, the optical properties can be remarkably improved or, on the contrary, degraded. This result opens promising perspectives towards the practical development of a double-function thermionic-thermal converter to be used in novel hybrid CSP plants.

It is worth to note that the idea we propose here, i.e. the use of a single engineered ceramic bulk to carry out both functions of absorber of concentrated solar radiation and TEC cathode, is radically different, significantly simpler and more robust and durable than the approach of the deposition of an electron emitting thin layer on a selective substrate [31] with consequent defects, adhesion and durability problems, making it applicable in the most advanced thermionic-based solutions found in the literature, such as combined thermionic-thermoelectric generators [32], and hybrid thermionic-photovoltaic converters [33]. For the same reasons of superior durability and reliability, the use of a bulk ceramics is advantageous for the solar absorbing function as well, in comparison to the alternative approach of deposing a solar absorbing coating on a substrate. In fact, at our operating temperatures, which are expected to be higher than 1200 K, solar selective coatings developed so far [34–37], including those made with thin layers of UHTC materials [38–41], cannot be used.

2. Experimental

The LaB_6 disc of 34 mm diameter, 2.9 mm thickness was sintered by hot pressing at 1900 °C, 40 MPa, with holding time of 15 min, starting from commercial powders (H.C. Starck). The density of the sintered body, evaluated with the Archimede's method, was 3.7 g/cm^3 [20], resulting in a relative density of 80 %. One surface of the disc was polished with diamond paste down to 1 μm. More details about the sample preparation are reported in [19].

The surface treatments were carried out by employing a Ti:Sapphire linearly polarized femtosecond laser (wavelength λ = 800 nm, pulse duration ~100 fs, repetition rate f = 1 kHz). The laser beam was focused perpendicularly on the surface of the sample, positioned on the motorized nanometric resolution stage of a Newport μFAB workstation. The treatments were performed by 12 mm × 12 mm of active area in air environment. The accumulated laser fluence is calculated as the product between the single pulse fluence (ϕ_P) and the number of pulses (equals to wf/v, being w the diameter of the laser spot and v the fabrication velocity). The laser spot diameter was assessed with the method described in Ref. [42].

The microstructure of the original polished sintered surface and of the laser-treated surfaces were analyzed using field emission gun-scanning electron microscope (FE-SEM, ZEISS Sigma, Carl Zeiss Microscopy GmbH, Germany) and energy dispersive X-ray spectroscopy (EDS, INCA Energy 300, Oxford instruments, UK).

Room-temperature hemispherical reflectance spectra were acquired using a double-beam spectrophotometer (Lambda900 by Perkin Elmer) with Spectralon®-coated integration sphere for the 0.3–2.5 μm wavelength region and a Fourier Transform spectrophotometer (FT-IR "Excalibur" by Bio-Rad) with gold-coated integrating sphere and liquid nitrogen-cooled detector for the range 2.5–16.0 μm. From experimental reflectance data ($R\cap(\lambda)$), the spectral absorbance $\alpha(\lambda)$ or emittance $\varepsilon(\lambda)$ of these fully opaque materials can be obtained, as:

$$\alpha(\lambda) = 1 - R\cap(\lambda) = \varepsilon(\lambda) \tag{1}$$

Then, a comparison among treated and untreated surfaces can be carried out by estimating the samples' solar absorptance α, the total hemispherical emittance ε at the temperature T, and the spectral selectivity α/ε, according to the following equations:

$$\alpha = \frac{\int_{0.3\mu m}^{3\mu m} \alpha(\lambda)\cdot S(\lambda) d\lambda}{\int_{0.3\mu m}^{3\mu m} S(\lambda) d\lambda} \tag{2}$$

$$\varepsilon = \frac{\int_{0.3\mu m}^{16.0\mu m} \varepsilon(\lambda)\cdot B(\lambda,T)d\lambda}{\int_{0.3\mu m}^{16.0\mu m} B(\lambda,T)d\lambda} \quad (3)$$

where S(λ) is the sunlight spectral distribution [43] and B(λ,T) is the blackbody spectral radiance at the temperature T. For a more complete evaluation, the emittance in Eq. (3) has been calculated at different temperatures from 800 K to 1930 K.

3. Results and discussion

Table 1 lists the investigated surfaces and their laser processing parameters. The accumulated laser fluence (ϕ) varies around 21 J/cm^2, which was evaluated as the threshold for obtaining LIPSS by preliminary experiments performed with single laser spot. Since the beam has a Gaussian shape, a proportional correlation between increase of the laser spot diameter and the average single pulse fluence is found. To obtain such value, the single pulse fluence and the total pulse number were changed accordingly to achieve similar ϕ. The sample appearance is shown in Fig. 1. The study is focused on the variation of the morphological and compositional properties obtained by changing ϕ_P and N and maintaining a fixed ϕ.

Features of the as sintered surface prior to the laser treatments are shown in Fig. 2. The ceramic contained a significant fraction of porosity, in agreement with density measurements, and the grain size ranged from 3 to 10 μm. Traces of La_x-O_y phases were detected along the grain boundaries by SEM-EDS analysis, Fig. 2b,c. These impurities are typical contaminants of boride powders and tend to segregate at the grain boundaries and triple points during densification, leaving white spurious pockets, see Fig. 2b.

It was previously observed that for other UHTCs, e.g. HfC, TaC and TaB_2 [13,25,44], the laser treatment always modified the surface morphology. For LaB_6, after treatment L3, a surface modification occurred but no ripples were formed and some traces of La_x-O_y phases were still detected, see Fig. 4c, f. On the contrary, after treatments L2 and L1 the surface patterning is evident as reported in Fig. 4b,e and 4 a, d. The periodic patterning, induced by linearly polarized pulses, and oriented perpendicularly to these, presents the typical unidimensional repetition of LIPSS. The spatial periodicities of the LIPSS were calculated by performing 2D Fast Fourier Transform (2D-FFT) onto the SEM micrographs presented in Fig. 3e and Fig. 3f. The software Gwyddion (v2.60) was used to calculate the two-dimensional histograms of the spatial frequencies in the original SEM images. Usually, 1D-LIPSS presents sickle-shaped features for which the center position determines the most frequent spatial periods, Λ [45]. Spatial periodicities of 615 ± 70 nm for L2 and 615 ± 50 nm for L1 were found after 2D-FFT and are shown in Fig. 3a and Fig. 3b respectively. The spatial periodicity ($\lambda/2 \leq \Lambda \leq \lambda$) and the orientation of LIPSS is consistent with Low Spatial Frequency LIPSS (LSFL) that can be found on highly absorbing materials, and are often classified as LSFL-I [46].

The formation or no-formation of ripples was observed to be connected with a very narrow threshold for the accumulated laser fluence.

Table 1
Investigated samples.

Surface label	Laser spot diameter (μm)	Single Pulse Fluence ϕ_P (J/cm^2)	Pulse number (N)	Accumulated laser fluence (J/cm^2)
L0 (untreated surface for reference)		——	——	——
L1	150	0.214(9)	100	21.49
L2	165	0.382(5)	55	21.04
L3	185	0.566(6)	37	20.96

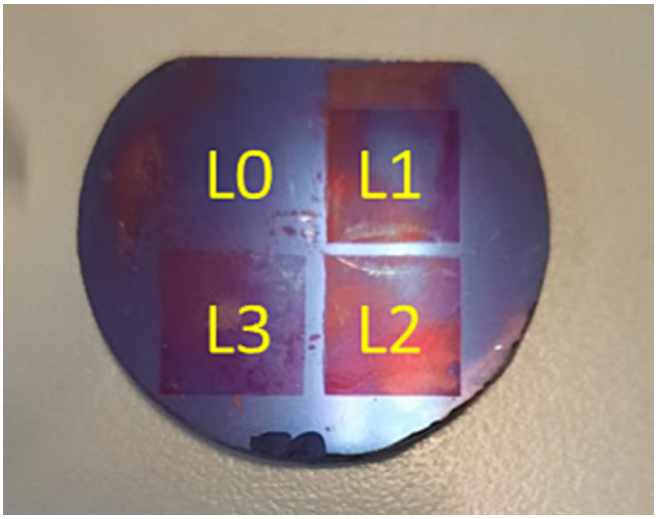

Fig. 1. Laser-processed LaB6 ceramic disk. L0: pristine untreated surface. L1-L3: treated surfaces.

In a previous work on HfC [44], ripples were not obtained with 7 J/cm^2 fluence, but were produced with 15 J/cm^2. Here, for LaB_6, the formation of ripples was observed at higher fluences than HfC, in agreement with the lower absorbance of LaB_6 at the laser wavelength, in comparison to the carbide. Another important parameter for the formation of LIPSS and their peak-to-valley depth is the number of pulses that impinge the surface. LIPSS formation is a multi-pulse phenomenon and an increasing number of pulses induces a positive feedback caused by the deepening of the grooves [46]. In this case, it is obvious that as the number of pulses increases, the LIPSS are more defined, as recently observed also for other materials considering a fixed single pulse fluence [47]. This is confirmed also for LaB_6 since, despite the highest single pulsed fluence (about 2.6 times more for L3 with respect to L1), the sample treated with a higher processing speed (i.e., lower number of impinging pulses) is the one presenting the less regular nanostructures, and only an embryonal form of LIPSS.

Compared to the as sintered surface, with roughness Ra of 0.08 ± 0.02 μm, the laser treatment increased the surface roughness in all the cases. The highest value was for treatment L1 with Ra = 0.27 ± 0.14 μm, whilst the measured roughness of L2 (with ripples) and L3 (with no ripples) were quite similar, Ra = 0.14 ± 0.08 μm and L3 Ra = 0.18 ± 0.07 μm, respectively. More difficult is to understand the effect of laser onto the pores and surface discontinuities. Generally speaking, the laser treatment seems to have partially removed secondary La-O phases detected in the as-sintered ceramic. The EDS analysis confirmed the presence of carbon in all surfaces.

The solar absorptance, thermal emittance and spectral selectivity, calculated from Eqs. (1)–(3), are shown in Fig. 5. In all cases, the treatments modify the surfaces' optical properties with respect to the pristine reference sample (L0) and always increase the solar absorptance. For L3 treated surface, the increase in solar absorptance is accompanied by an increase of the thermal emittance as well. However, remarkably, in the cases of L1 and L2 surfaces, the laser texturing also decreases the thermal emittance at the same time, resulting therefore in the improved spectral selectivity. This is a very promising result towards the practical application of these materials as high-temperature CSP solar absorbers, and, to the best of our knowledge, it is the first demonstration of solar-selectivity enhancement by ultra-short pulsed laser processing in ceramic solar thermodynamic absorbers.

The obtained results of optical parameters could be explained as an interplay between two different effects: the laser-induced changes in surface composition and changes in surface morphology (presence of ripples and their spacing). If we consider the couple of treatments L1 and

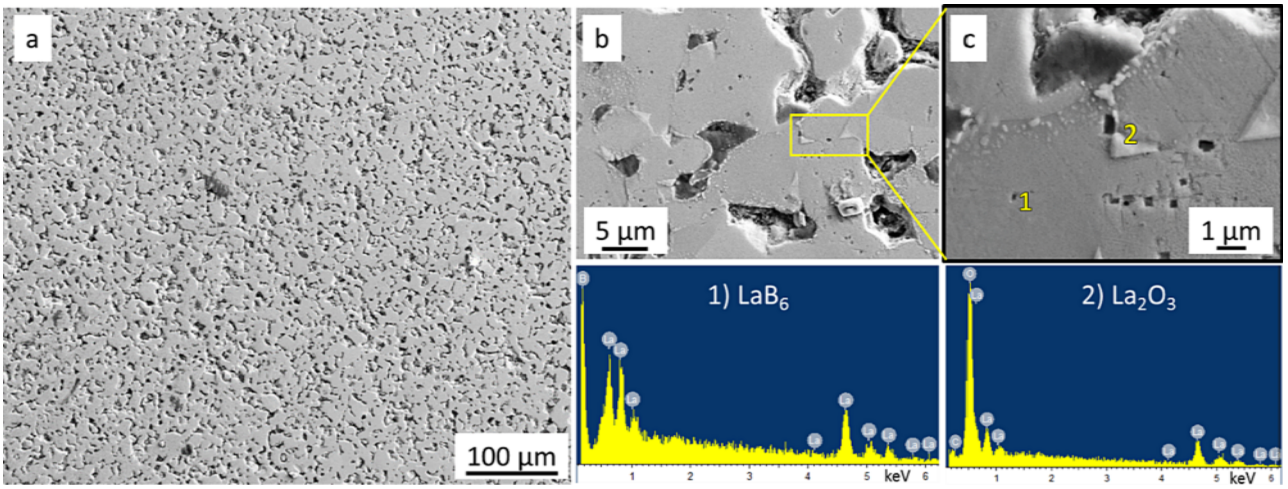

Fig. 2. a) SEM image showing microstructure of as sintered surface (L0). b-c) SEM images showing presence of traces of La_2O_3 phase detected by EDS analysis (spectrum 2).

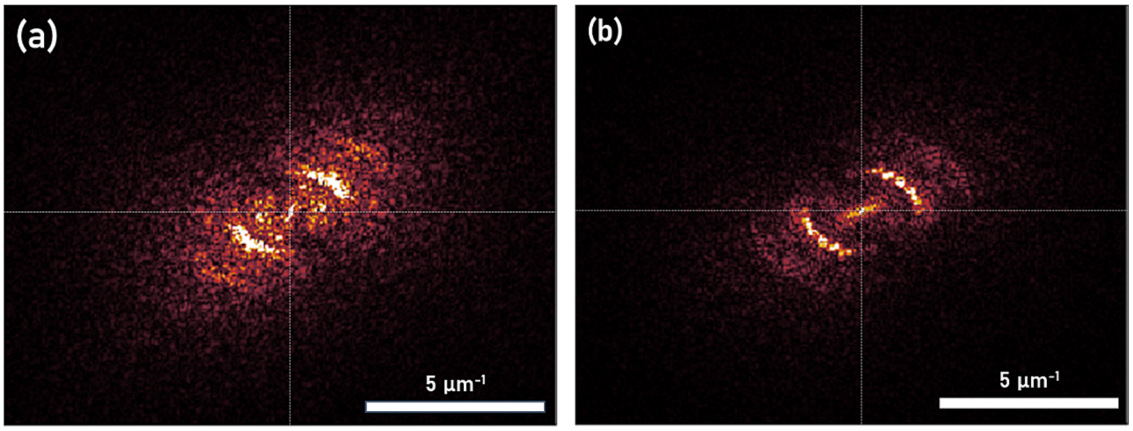

Fig. 3. a) 2D-FFT of sample L2. b) 2D-FFT of sample L1. In this picture it is possible to denote a lower dispersion of spatial frequencies around the peak centered at 1.626 μm^{-1}.

L2, we see that L2 has a slightly higher solar absorptance. According to the approach given in [13], this is consistent with the slightly larger size distribution of LIPPS in L2, entailing a slightly higher value of solar irradiance integral in the range of L2 ripples. In other words, the slightly higher solar absorptance found in L2 is due the trapping of a slightly larger portion of solar spectrum. On the other hand, also the L3 sample shows an increased solar absorptance with respect to L0, but lower than L1, L2: the trapping of solar radiation is very weak in L3 due to the presence of few embryonal LIPPS.

As for the emittance trend, the partial removal of the high-emittance oxide phases [48] by the heaviest laser treatments could explain the lower thermal emittance of L1 and L2 with respect to the pristine sample, as the laser-induced features on the surfaces are much smaller than thermal radiation wavelengths. For L3, the increased emittance with respect to L0 could be due to the appearance of embryonal LIPPS in a non-homogeneous way on the surface, which induces larger-scale superstructures of sizes compatible with thermal radiation wavelengths. Finally, even if further investigations are needed to explain the emittance difference between L1 and L2, we could, however, hypothesize that the different stoichiometric content on the two surfaces (proved from the color differences from blue to purple [49] seen in Fig. 1) could be related to the observed results.

As a side comments, it is worth to discuss that the values of optical parameters reported here and calculated from Eqs. (1)–(3), being obtained from room-temperature spectra, must be considered as estimated values, useful for comparisons among samples and generally underestimated with respect to the values measured on heated samples [11,19]. They agree with the similarly calculated values on the untreated porous and polished LaB_6 ceramic in Ref. [4], whose experimentally measured thermal emittance at 1100 K was found to be around 0.4 [4] and was used in [20] to calculate the expected solar-to-electric conversion efficiency of LaB_6 double-function ceramic TEGs.

According to these estimations, a prediction under ideal conditions of the solar-to-thermal conversion efficiency ($\eta_{s\text{-}th}$) can be done to compare the results of L2 and L0 samples (Fig. 6a) to act as selective solar absorber. $\eta_{s\text{-}th}$ is calculated as:

$$\eta_{s-th} = \alpha - \varepsilon(T)\cdot\frac{\sigma \times T^4}{C \times I} \quad (4)$$

where σ is the Stefan-Boltzmann constant, C is the solar concentration ratio and I is the average solar irradiance (1 kW/m^2).

At the fixed value of C = 400, a value that can be obtained in the solar tower architecture [50], we found that the treated sample shows an improvement of $\eta_{s\text{-}th}$ in all the investigated range of temperature up to an increase of 9 % at T = 1930 K, even if the maximum value of 60.6 % is reached at T = 800 K. On the other side, by varying the value of C, $\eta_{s\text{-}th}$ increases when the operative temperature is lower, and C is higher (Fig. 6b). The maximum value of 60.6 % efficiency is reached for L2 sample when T = 1000 K and C = 1000 suns, much higher than that of

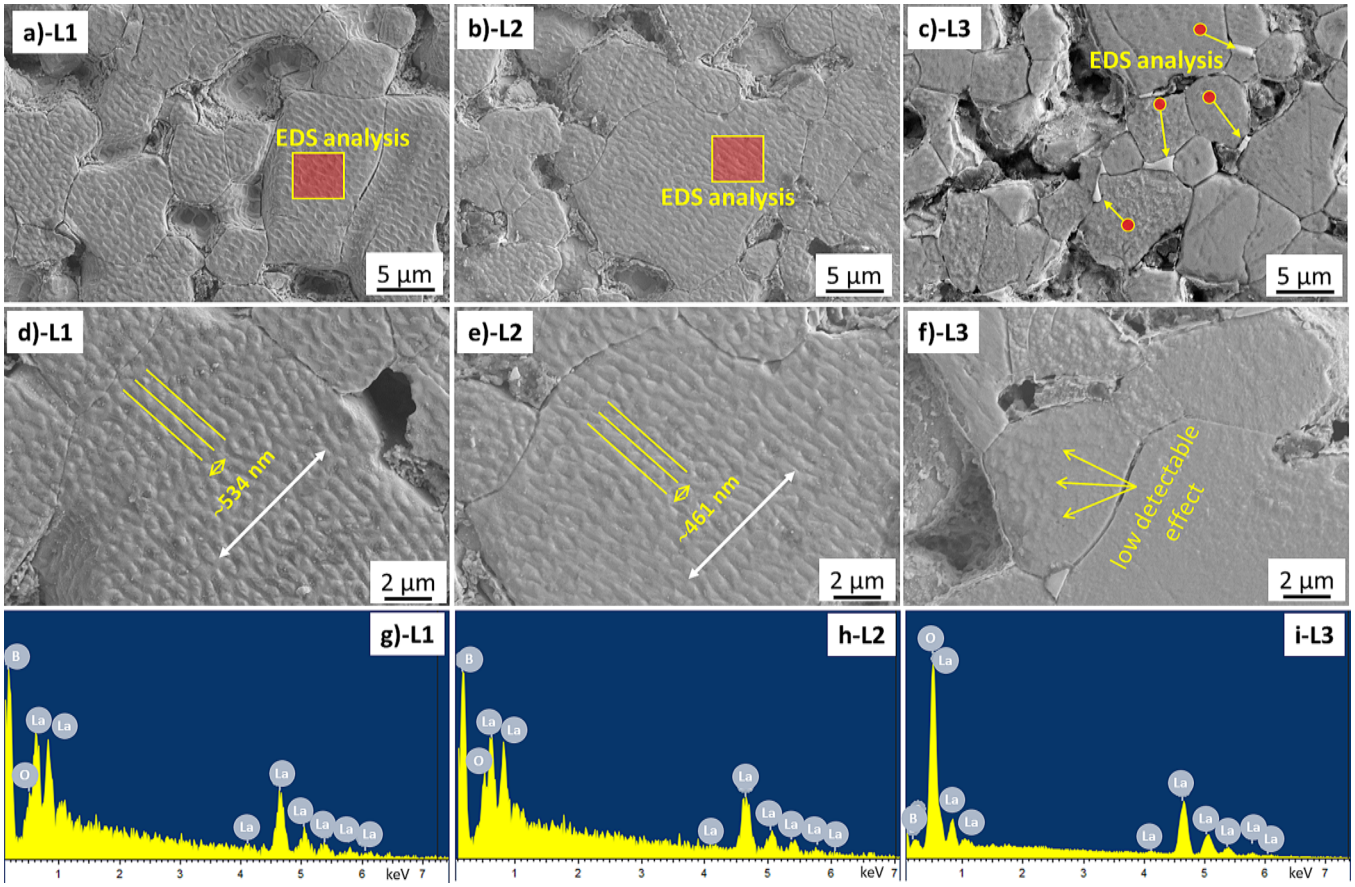

Fig. 4. SEM images of the microstructures of treated surfaces (From left to right: L1, L2, L3) highlighting the variation of the laser treatment. The periodic spacings on the f)-L3 surface were not detectable. The direction of the laser polarization (i.e. normal to the LIPSS) is indicated by the white arrows in d)-L1 and e)-L2 images. The EDS spectra g-i) are referred to the areas indicated in a-c.

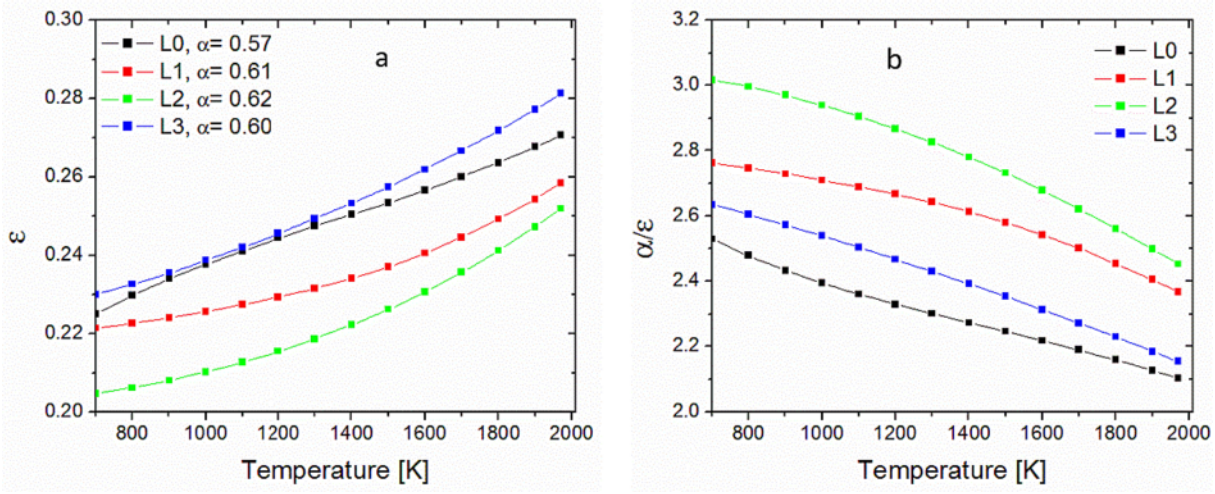

Fig. 5. Calculated thermal emittance (a) and spectral selectivity (b) as a function of temperature. The calculated solar absorptance values are indicated in legend.

SiC (efficiency ~ 50 % [51]), which is, to date, the most advanced bulk absorber material used in existing CSP plants [51,52]. Additionally, $\eta_{s\text{-}th}$ showed little variations when the concentration ratio increases at the lowest considered temperatures ~ 1000–1200 K, whereas when the temperature increases, the dependence of photothermal efficiency on the solar concentration ratio becomes more pronounced. At the maximum considered temperature of 1930 K, the photothermal efficiency is 29.1 % for C = 600 and 42.2 % for C = 1000.

On the other hand, as introduced before, LaB_6 is a well-known material to be used in thermionic converters, since it can act as engineered absorber able to both produce electricity and feed a secondary thermal stage like heat transfer fluids (HTF) and then turbines. With the aim to have a more realistic and reliable estimation of the performance of treated LaB_6 samples as cathodes in solar thermionic converters, a finite-element model by COMSOL Multiphysics v5.6 was performed to predict the temperature of a laser-treated LaB_6 disc with a diameter of 100 cm.

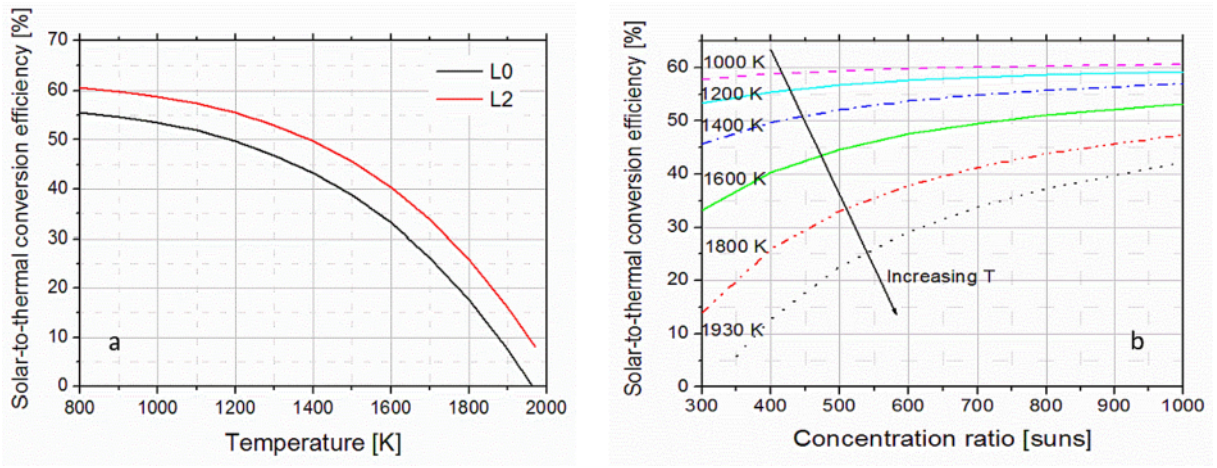

Fig. 6. Evaluation of the performance of the treated sample L2 vs the untreated L0 as selective solar absorber in terms of solar-to-thermal conversion efficiency as a function of operating temperature (a) and, for L2, as a function of the concentration ratio at fixed temperatures (b).

This size is considered as appropriated for the design of a converter to be installed in a CSP solar tower plant and parabolic dishes, where high values of C are managed. Therefore, a concentration ratio of 600 suns is fixed as the average value for central receiver systems [53].

The absorber is simulated in operating conditions, within a vacuum enclosure, illuminated by the concentrated sunlight passing a high transmittance quartz window and fixed to a molybdenum frame acting also as electrical contact for the converter. In these conditions, the temperature of the absorber is 1930 K (Fig. 7), which is a value considerably lower than that needed for materials typically used in the thermionic energy conversion (e.g., refractory metals).

Based on these estimations and considering the work function and the Richardson constant measured in [20], equal to 2.55 eV and 43.62 A/cm^2K^2, respectively, we can calculate the solar-to-electrical conversion $\eta_{s\text{-}e}$ of the thermionic conversion stage as:

$$\eta_{s-e} = \eta_{therm} = \frac{J \times V}{C \times I} \tag{5}$$

being η_{therm} the thermionic conversion efficiency, J the net thermionic current density and V the converter output voltage. Fig. 8 shows $\eta_{s\text{-}e}$ calculated as a function of different anode work function Φ_A (with a Richardson constant of 120 A/cm^2K^2) when the temperature difference between anode and cathode is fixed to 500 K, that is a reasonable value allowing for the exploitation of a residual thermal flux with HTF and a second conversion cycle. The space-charge effects are considered negligible, supposing the inter-electrode distance is maintained optimal with the use of technological solutions specifically developed for this aim [54,55].

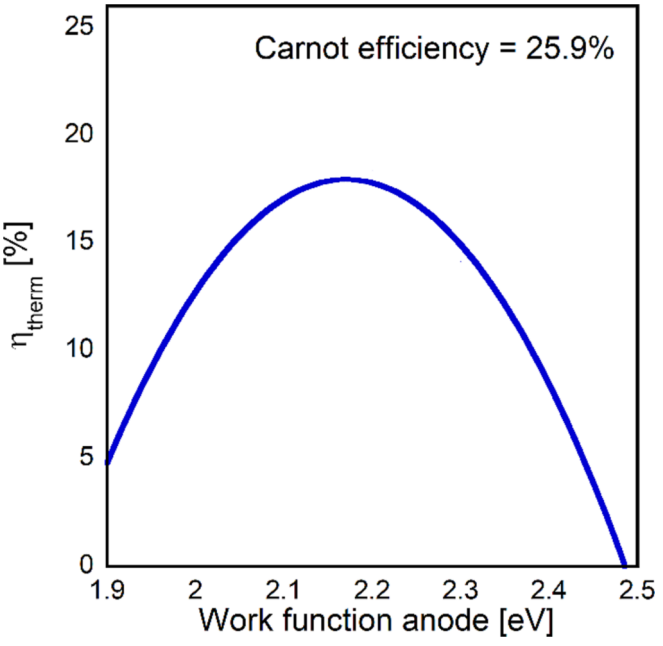

Fig. 8. Thermionic conversion efficiency as a function of the anode work function.

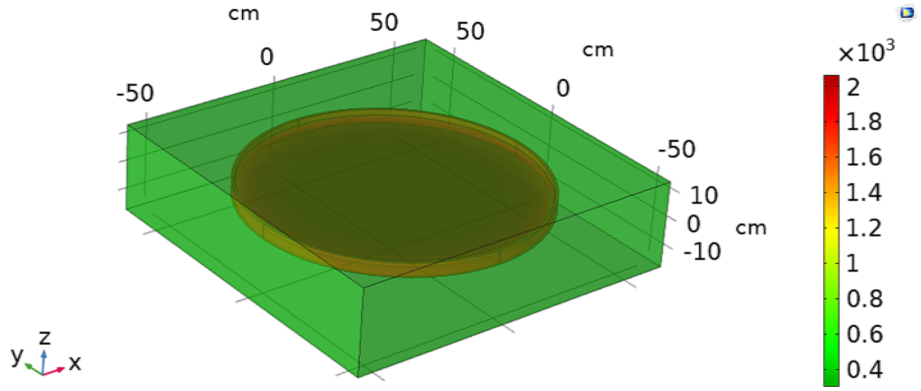

Fig. 7. Simulated temperature distribution in the sunlight-irradiated LaB_6 ceramics.

We found that the maximum value of the conversion efficiency is18.4 % when the Φ_A is 2.2 eV, close to maximum conversion efficiency due to the Carnot limit. The trend can be explained in a simple way: on one side, when Φ_A is lower than the optimal value, η_{therm} decreases since the anode counter-emission is too strong; on the other side, a value of Φ_A higher than 2.2 eV leads to a very low output voltage, thus decreasing the thermionic power. This estimation represents a very promising value, because of this engineered receiver could produce 70.0 kW of electricity (considering an active area for the cathode of 6358 cm^2) and, at the same time, contributing to feed a secondary thermal flux with the anode at a temperature of 1430 K.

4. Conclusions

To develop novel double-function solar thermal absorbers/thermionic cathodes operating at high temperatures, sintered ceramics of LaB_6 were treated by femtosecond laser. It was found that, depending on the treatment parameters, the ceramic surface was modified in different ways. Surface roughness was increased in all cases, while Laser Induced Periodic Surface Structures (LIPSS) were created only for specific values of single pulse fluence and number of pulses, which induce a very defined window in terms of accumulated laser fluence. In addition, SEM analysis detected the partial removal of oxide phases on the laser-treated surfaces. As a consequence of both effects, the optical properties were strongly changed: the solar absorptance was always increased. For the two samples showing LIPSS, this was also accompanied by a decrease of thermal emittance, entailing thus an increased spectral selectivity, which is a remarkable result for the intended high-temperature solar absorber application. An about 9 % increase of the estimated solar-to-thermal conversion efficiency was found for the best treated surface, with respect to the as-sintered sample, for C = 400 concentration ratio. Efficiency values from 57.8 % to 60.6 % were predicted in the range 300–1000 of concentration ratio when the temperature is 1000 K. As the operating temperature is increased, the photothermal efficiency of the absorbers physiologically decreases and the dependence on the solar concentration ratio becomes more marked. At the maximum considered temperature of 1930 K, the photothermal efficiency is 29.1 % for C = 600 and 42.2 % for C = 1000.

Additionally, the performances of LaB_6 treated discs as thermionic cathodes were assessed by multiphysics modelling under simulated operative conditions of C = 600 and 1930 K temperature. A maximum solar-to-electrical conversion efficiency of the thermionic stage of as much as 18.4 %, not far to the Carnot efficiency limit (25.9 %), is calculated. The heat rejected by the anode towards a cascaded thermal or thermodynamic stage in this case has a temperature of 1430 K. These results open interesting perspectives towards the development of an efficient double-function ceramic bulk material to be used as direct power converter and high-temperature solar absorber element for Concentrating Solar Power and Concentrating Solar Thermal.

CRediT authorship contribution statement

Elisa Sani: Conceptualization, Methodology, Investigation, Validation, Data curation, Writing – original draft, Writing – review & editing, Visualization, Funding acquisition, Supervision. **Diletta Sciti:** Methodology, Writing – review & editing. **Simone Failla:** Investigation, Visualization, Writing – review & editing. **Alessandro Bellucci:** Methodology, Investigation, Visualization, Writing – review & editing. **Matteo Mastellone:** Investigation, Visualization, Writing – review & editing. **Stefano Orlando:** Investigation. **Daniele M. Trucchi:** Methodology, Writing – review & editing.

Declaration of competing interest

The authors declare that they have no known competing financial interests or personal relationships that could have appeared to influence the work reported in this paper.

Acknowledgements

This study was partially developed in the framework of the research activities carried out within the Project "Network 4 Energy Sustainable Transition—NEST", Spoke 1, Project code PE0000021, funded under the National Recovery and Resilience Plan (NRRP), Mission 4, Component 2, Investment 1.3— Call for tender No. 1561 of 11.10.2022 of Ministero dell'Universita'e della Ricerca (MUR); funded by the European Union—NextGenerationEU. The CNR-INO technicians Mauro Pucci and Massimo D'Uva are acknowledged for technical support, as well as CNR-INO administration staff Francesca Usala, Pasqualina Pipino and Roberta Parenti.

References

[1] C. Murphy, Y. Sun, W. Cole, G. Maclaurin, C. Turchi, M. Mehos, The potential role of concentrating solar power within the context of DOE's 2030 solar cost targets, Technical (2019).
[2] *World Energy Outlook 2021*. International Energy Agency.
[3] R. Thonig, J. Lilliestam, Concentrating Solar Technology Policy Should Encourage High Temperatures and Modularity to Enable Spillovers., *AIP Conf. Proc.*, vol. in review, p. www.solarpaces.org/wp-content/uploads/Conc, 2021.
[4] R. Schäppi, et al., Drop-in fuels from sunlight and air, Nature 601 (2022) 63–68.
[5] S. Zoller, et al., A solar tower fuel plant for the thermochemical production of kerosene from H2O and CO2, Joule 6 (2022) 1606–1616.
[6] E. Sani, L. Mercatelli, M. Meucci, L. Silvestroni, A. Balbo, D. Sciti, Process and composition dependence of optical properties of zirconium, hafnium and tantalum borides for solar receiver applications, Sol. Energy Mater. Sol. Cells 155 (2016) 368–377.
[7] E. Sani, L. Mercatelli, M. Meucci, A. Balbo, L. Silvestroni, D. Sciti, Compositional dependence of optical properties of zirconium, hafnium and tantalum carbides for solar absorber applications, Sol. Energy 131 (2016) 199–207, https://doi.org/10.1016/j.solener.2016.02.045.
[8] W. Fahrenholtz, A historical perspective on research related to ultra-high temperature ceramics, in: Ultra-High Temperature Ceramics: Materials for Extreme Environment Applications, John Wiley & Sons Ltd, 2014, p. 21.
[9] E. Sani, et al., Optical properties of dense zirconium and tantalum diborides for solar thermal absorbers, Renew. Energy 91 (2016), https://doi.org/10.1016/j.renene.2016.01.068.
[10] E. Sani, E. Landi, D. Sciti, V. Medri, Optical properties of ZrB2 porous architectures, Sol. Energy Mater. Sol. Cells 144 (2016) 608–615, https://doi.org/10.1016/j.solmat.2015.09.068.
[11] N. Azzali, et al., Spectral emittance of ceramics for high temperature solar receivers, Sol. Energy 222 (2021) 74–83.
[12] L. Silvestroni, D. Sciti, L. Zoli, A. Balbo, F. Zanotto, R. Orrù, R. Licheri, C. Musa, L. Mercatelli, Sani, An overview of ultra-refractory ceramics for thermodynamic solar energy generation at high temperature, Renew. Energy 133 (2019) 1257–1267.
[13] E. Sani, D. Sciti, L. Silvestroni, A. Bellucci, S. Orlando, D.M. Trucchi, Tailoring optical properties of surfaces in wide spectral ranges by multi-scale femtosecond-laser texturing: a case-study for TaB2 ceramics, Opt. Mater. (Amst) 109 (2020) 110347.
[14] E. Sani, D. Sciti, S. Failla, C. Melandri, A. Bellucci, D. Trucchi, Multi-scale femtosecond-laser texturing for photothermal efficiency enhancement on solar absorbers based on TaB2 ceramics, Nanomaterials 13 (2023) 1692, https://doi.org/10.3390/nano13101692.
[15] A. Santagata, et al., Enhanced and selective absorption of molybdenum nanostructured surfaces for concentrated solar energy applications, Materials (Basel) 15 (2022) 8333.
[16] J.M. Lafferty, Boride cathodes, J. Appl. Phys. 22 (1951) 299–309.
[17] A.N. Broers, Some experimental and estimated characteristics of the lanthanum hexaboride rod cathode electron gun, J. Phys. E 2 (1969) 273.
[18] A.N. Broers, High-resolution thermionic cathode scanning transmission electron microscope, Appl. Phys. Lett. 22 (1973) 610–612.
[19] E. Sani, L. Mercatelli, M. Meucci, L. Zoli, D. Sciti, Lanthanum hexaboride for solar energy applications, *Sci. Rep.*, 7(10) (2017), doi: 10.1038/s41598-017-00749-w.
[20] A. Bellucci, et al., Thermionic emission measurement of sintered lanthanum hexaboride discs and modelling of their solar energy conversion performance, Ceram. Int. 47 (2021) 20736–20739, https://doi.org/10.1016/j.ceramint.2021.04.079.
[21] J.I. Gittleman, E.K. Sichel, H.W. Lehmann, R. Widmer, Textured silicon: A selective absorber for solar thermal conversion, Appl. Phys. Lett. 35 (1979) 742–744.
[22] J. Li, H. Yu, Y. Li, F. Wang, M. Yang, S.M. Wong, Low aspect-ratio hemispherical nanopit surface texturing for enhancing light absorption in crystalline Si thin film-based solar cells, Appl. Phys. Lett. 98 (2011) 021905.
[23] R. Jain, R. Pitchumani, Fabrication and characterization of multiscale, fractal textured solar selective coatings, Sol. Energy Mater. Sol. Cells 172 (2017) 213–219.
[24] K. Kant, K.P. Sibin, R. Pitchumani, Novel fractal-textured solar absorber surfaces for concentrated solar power, Sol. Energy Mater. Sol. Cells 248 (2022) 112010.

[25] D. Sciti, D.M. Trucchi, A. Bellucci, S. Orlando, L. Zoli, E. Sani, Effect of surface texturing by femtosecond laser on tantalum carbide ceramics for solar receiver applications, Sol. Energy Mater. Sol. Cells 161 (2017), https://doi.org/10.1016/j.solmat.2016.10.054.
[26] N. Zhou, et al., Controllable preparation of microtips array on (100) crystal plane of single-crystal lanthanum hexaboride ceramic, J. Am. Ceram. Soc. 105 (2022) 1896–1903.
[27] M. Birnbaum, Semiconductor surface damage produced by ruby lasers, J. Appl. Phys. 36 (1965) 3688–3689.
[28] A.Y. Vorobyev, V.S. Makin, C. Guo, Periodic ordering of random surface nanostructures induced by femtosecond laser pulses on metals, J. Appl. Phys. 101 (2007) 34903.
[29] M. Mastellone, et al., LIPSS applied to wide bandgap semiconductors and dielectrics: assessment and future perspectives, Materials (Basel) 15 (2022) 1378.
[30] C. Florian, S.V. Kirner, J. Krüger, J. Bonse, Surface functionalization by laser-induced periodic surface structures, J. Laser Appl. 32 (2020) 022063.
[31] A. Bellucci, et al., Nanocrystalline lanthanum boride thin films by femtosecond pulsed laser deposition as efficient emitters in hybrid thermionic-photovoltaic energy converters, Appl. Surf. Sci. 513 (February) (2020) 145829, https://doi.org/10.1016/j.apsusc.2020.145829.
[32] D.M. Trucchi, et al., Solar thermionic-thermoelectric generator (ST2G): concept, materials engineering, and prototype demonstration, Adv. Energy Mater. 8 (32) (2018) 1802310, https://doi.org/10.1002/aenm.201802310.
[33] A. Datas, Hybrid thermionic-photovoltaic converter, Appl. Phys. Lett. 108 (2016) 143503.
[34] K.P. Kumar, S. Mallick, S. Sakthivel, Cobalt-rich spinel oxide-based wide angular spectral selective absorber coatings for solar thermal conversion applications, Renew. Energy 203 (2023) 334–344.
[35] Z.Y. Nuru, C.J. Arendse, N. Mongwaketsi, S.K. Gohshal, M. Nkosi, M. Maaza, Effects of substrate temperatures on the thermal stability of AlxOy/Pt/AlxOy multilayered selective solar absorber coatings, Renew. Energy 75 (2015) 590–597.
[36] A. Al-Rjoub, et al., A design of selective solar absorber for high temperature applications, Sol. Energy 172 (2018) 177–183.
[37] K.P. Sibin, K. Kant, R. Pitchumani, High-temperature air stability of electrodeposited copper cobalt oxide and copper manganese oxide absorber coatings for concentrating solar power, ACS Appl. Energy Mater. 6 (2023) 8759–8774.
[38] S. Zhao, et al., High-entropy alloy nitride AlMo0. 5NbTa0. 5TiZrN x-based high-temperature solar absorber coating: structure, optical properties, and thermal stability, ACS Appl. Energy Mater. 5 (2022) 9214–9224.
[39] C.Y. He, et al., Medium-entropy nitride ZrNbMo-WN nanofilm-based substrate-independent selective solar absorber by a cosputtering method, ACS Appl. Energy Mater. 5 (2022) 11517–11525.
[40] J. Wang, et al., High-performance spectrally selective absorber using the ZrB2-based all-ceramic coatings, ACS Appl. Mater. Interfaces 13 (2021) 40522–40530.
[41] S.S. Zhao, X.L. Qiu, C.Y. He, D.M. Yu, G. Liu, X.H. Gao, Nanometer-thick high-entropy alloy nitride Al0.4Hf0.6NbTaTiZrN based solar selective absorber coatings, ACS Appl. Nano Mater. 4 (2021) 4504–4512.
[42] M. Mastellone, et al., Enhanced selective solar absorption of surface nanotextured semi-insulating 6H–SiC, Opt. Mater. (Amst) 107 (2020) 109967.
[43] Standard Tables for Reference Solar Spectral Irradiances: Direct Normal and Hemispherical on 37° Tilted Surface, Active Standard ASTM G173. ASTM G173 - 03, (2012).
[44] D. Sciti, L. Silvestroni, D.M. Trucchi, E. Cappelli, S. Orlando, E. Sani, Femtosecond laser treatments to tailor the optical properties of hafnium carbide for solar applications, Sol. Energy Mater. Sol. Cells 132 (2015), https://doi.org/10.1016/j.solmat.2014.09.037.
[45] J. Bonse, Quo vadis LIPSS?—Recent and future trends on laser-induced periodic surface structures, Nanomaterials 10 (1950) (2020), https://doi.org/10.3390/nano10101950.
[46] J. Bonse, S. Gräf, Maxwell meets Marangoni—A review of theories on laser-induced periodic surface structures, Laser Photon. Rev. 14 (2020) 2000215.
[47] M. Mastellone, et al., Surface nanotexturing of boron-doped diamond films by ultrashort laser pulses, Micromachines 14 (2023) 389.
[48] M.F. Modest, S. Mazumder, Radiative Heat Transfer, 4th edition, Academic Press, 2021.
[49] M.J. McKelvy, L. Eyring, E.K. Storms, Analytical and structural analysis of the lanthanum-deficient lanthanum hexaboride, J. Phys. Chem. 88 (1984) 1785–1790.
[50] B. Belgasim, Y. Aldali, M.J. Abdunnabi, G. Hashem, K. Hossin, The potential of concentrating solar power (CSP) for electricity generation in Libya, Renew. Sustain. Energy Rev. 90 (2018) 1–15.
[51] K. Burlafinger, A. Vetter, C.J. Brabec, Maximizing concentrated solar power (CSP) plant overall efficiencies by using spectral selective absorbers at optimal operation temperatures, Sol. Energy 120 (2015) 428–438.
[52] V. Casalegno, et al., SiC–based solar receivers for CSP: component manufacturing and joining, Materials (basel) 14 (2021) 4687.
[53] M.I. Roldán Serrano, Concentrating solar thermal technologies, in: M.I. Roldán Serrano (Ed.), Concentrating Solar Thermal Technologies: Analysis and Optimisation by CFD Modelling, Springer International Publishing, 2017, pp. 11–24.
[54] S.M. Nicaise, et al., Micron-gap spacers with ultrahigh thermal resistance and mechanical robustness for direct energy conversion, Microsyst. Nanoeng. 5 (2019) 31.
[55] A. Bellucci, et al., Dielectric micro- and sub-micrometric spacers for high-temperature energy converters, Energy Technol. 9 (1) (2021) 2000788, https://doi.org/10.1002/ente.202000788.